https://doi.org/10.5194/egusphere-2026-1032
Preprint. Discussion started: 30 March 2026
© Author(s) 2026. CC BY 4.0 License.

Physical Constrained Retrieval of Fog Visibility from Millimeter-Wavelength Cloud Radar Observations

Xiaojie Li[1], Jinming Ge[1], Yucheng Qiu[1], Qiaoyi Lv[2], Wei Song[3], Jie Zhang[1], Chi Zhang[1], Bochun Liu[1], Jiapeng Wang[1], Hongwei Xia[1], and Yuhang Zhu[1]

[1]Key Laboratory for Semi-Arid Climate Change of the Ministry of Education and the College of Atmospheric Sciences, Lanzhou University, Lanzhou, 730000, China
[2]Xiamen Key Laboratory of Straits Meteorology, Xiamen, 361012, China
[3]Tianjin Weather Modification Office, Tianjin, 300061, China

Correspondence: Jinming Ge (gejm@lzu.edu.cn) and Qiaoyi Lv (414562004@qq.com)

Abstract. Fog severely degrades visibility (Vis) and poses substantial risks to transportation and aviation, yet its quantitative monitoring remains challenging, because conventional optical and passive remote sensing techniques lose sensitivity under dense fog conditions. Millimeter-wave cloud radar (MMCR) provides a promising alternative due to its strong penetration capability and fine spatial resolution; however existing Vis retrieval algorithms largely rely on empirical parameterizations, resulting in considerable uncertainties. In this study, we develop a physically constrained fog Vis retrieval framework that explicitly links radar reflectivity(Z) to fog microphysical properties through radiative transfer theory. Visibility is inferred by estimating the extinction coefficient from independently derived fog liquid water content (LWC) and effective droplet radius (re), thereby avoiding purely empirical formulations. The method is applied to a Ka band MMCR observations at the Datan Observation Base (DOB) Fujian province, China. LWC is retrieved using a mass-absorption based algorithm developed in our previous study. A power-law relationship between the geometric mean radius (rm) and radar reflectivity (Z) is then established using 5 years of droplet size distribution data from an FM-120 fog droplet spectrometer, enabling a reasonable estimation of re from observation. Based on the obtained LWC and droplet size parameters, the extinction coefficient (βext) and Vis are subsequently derived. Validation against ten sea-fog events in spring 2025 demonstrates that the proposed algorithm achieves a fractional error of 36.61%, outperforming commonly used empirical approaches, which exhibit errors ranging from 38.61% to 77.08%. These results indicate that our proposed framework provides a more reliable and physically interpretable solution for high-precision fog visibility retrieval using single-frequency MMCR observations.

1 Introduction

Fog, an atmospheric phenomenon, forms when moist air near the surface becomes saturated and condenses to water droplets that can significantly reduce horizontal visibility (Vis) often below 1 km. It is highly prevalent in valley, mountainous, urban and coastal regions, where radiative cooling, moisture advection, evaporation, or orographic lifting lead the near-surface air to reach saturation. It poses substantial risks to port operations, maritime traffic safety, and regional economic activities (Gultepe et al., 2009; Leung et al., 2020; Duran-Rosal et al., 2018). Vis, the core parameter for quantifying fog intensity and guiding

https://doi.org/10.5194/egusphere-2026-1032
Preprint. Discussion started: 30 March 2026
© Author(s) 2026. CC BY 4.0 License.

operational decisions, is defined as the maximum horizontal distance at which an observer with normal eyesight can distinguish a target against its background under current weather conditions (Long et al., 2021; Miclea et al., 2020). Despite its operational importance, accurately measuring Vis and characterizing fog structure remain challenging due to the limitations in existing observational techniques.

Various instruments have been used to conduct fog observations. Ground-based sensors such as optical visibility meters and fog droplet spectrometers provide high-precision point measurements but fail to capture the horizontal or vertical distribution of fog (Tjugum et al., 2005; Cheng et al., 2018; Zhou et al., 2024). Laser-based active remote-sensing instruments (e.g., lidar, ceilometers) offer vertical profiling capabilities; however, their signals suffer severe attenuation in dense fog, often leading to signal saturation or complete loss (Zang et al., 2019). Satellite passive imagers enable large-scale fog detection but struggle to distinguish fog from low-level clouds and lack vertical resolution to resolve internal stratification or microphysical structures (Ran et al., 2022; Guo et al., 2021). These limitations hinder reliable short-term fog nowcasting and proactive risk mitigation in transportation and maritime operations (Mahdavi et al., 2024; Antoine et al., 2023; Kamangir et al., 2022; Gultepe et al., 2007). In recent years, millimeter-wave cloud radar (MMCR) has gained prominence in fog monitoring due to its strong penetration, fine spatiotemporal resolution, and sensitivity to small hydrometeors. Field campaigns such as the 2021 Pingtan Sea Fog Experiment in China's Fujian Province have shown that Ka-band radar maintains robust signal integrity under dense fog conditions (Hu et al., 2022). Bell (2021) utilized dual-frequency radar to observe multi-layer fog, and by assimilating these radar data into the Applications de la Recherche à l'Opérationnel à Méso-Echelle (AROME) model, they reduced the fog-top height error by 64% and largely improved visibility forecasts. The development of millimeter-wave radar has thus provided a new means for fog detection.

Previous studies have made advancement in quantifying fog visibility. Many existing works aim to improve the conversion and simulation of fog visibility by establishing the relationship between fog microphysical properties and Vis based on their physical definitions. Early work by Eldridge (1966) proposed an inverse relationship between Vis and fog liquid water content (LWC) through bulk microphysical analysis, laying the foundation for empirical Vis modeling. Subsequent research demonstrated that droplet size distribution (DSD) strongly modulates extinction and visibility, motivating the development of more sophisticated models. For example, Gultepe et al. (2006) incorporated droplet number concentration (N) into a multi-parameter scheme, improving Vis estimates in Numerical Weather Prediction (NWP) models by up to 50%. Song et al. (2019) further enhanced Vis retrieval performance by integrating effective droplet diameter. Collectively, these studies indicate that incorporating fog microphysical properties can substantially improve the accuracy and physical consistency of Vis estimation (Ui et al., 2023; Jayakumar et al., 2025; Claxton, 2025). Despite these advances, most current radar-based Vis parameterizations remain largely empirical, typically derived by directly fitting Vis to radar reflectivity (Z) (Gultepe et al., 2009). Although Yunlong Li et al. (2017) introduced radar attenuation correction to obtain more accurate Z, the resulting Vis retrieval still relies primarily on empirical relationships. More recent radar-based approaches have begun to account for microphysical influence; however, they generally rely on auxiliary instruments to provide key supplementary information such as attenuation measurement or detailed fog microphysical parameters. This reliance on additional observations significantly restricts operational flexibility

https://doi.org/10.5194/egusphere-2026-1032
Preprint. Discussion started: 30 March 2026
© Author(s) 2026. CC BY 4.0 License.

and constrains the applicability in environments where supporting instrumentation is unavailable, thereby hindering robust fog detection and monitoring under practical conditions.

In this study, we develop a fog Vis retrieval algorithm for single-wavelength MMCR. Building on radar transmission theory and fog microphysics, we established quantitative physical linkages among Z, fog microphysical parameters—LWC, effective radius (r_e), and the extinction coefficient (β_{ext}, a 2nd moment parameter). This new physically constrained framework does not rely on empirical coefficients, therefore largely reduces the errors introduced by traditional methods and substantially improves adaptability and stability across a wide range of fog conditions, enabling accurate Vis estimation. The observational instruments and theoretical basis of the proposed retrieval algorithm are described in Sections 2 and 3, respectively. Section 4 analyzes method sensitivity to key parameters using data from fog droplet spectrometer monitor (FM-120) manufactured by the Droplet Measurement Technology company. Section 5 evaluates the algorithm's performance using a typical sea-fog case and statistical validation across ten sea fog cases. Section 6 finally summarizes the major findings and implications for operational fog monitoring.

2 Instrumentation and data

The Datan Observation Base (DOB) is located on Dadeng Island, Xiamen ($24.55°\mathrm{N}, 118.32°\mathrm{E}$) within the Taiwan Strait and surrounded by ocean on three sides. The site is operated by the Xiang'an District Meteorological Bureau (XDMB) under the Fujian Meteorological Bureau (FMB) and is situated in one of China's most fog-prone coastal areas. Positioned within a transition zone between marine and continental climates, this area frequently experiences interactions of warm, moist marine air masses and cold air, creating highly favorable conditions for sea fog formation (Zhang et al., 2024, 2023; Niu et al., 2010). Dedicated sea-fog monitoring campaigns have been conducted at DOB since 2019, yielding five years of fog observations that provide a valuable foundation for this study. Three specialized instruments are deployed at DOB for fog observation and analysis. The YLUKA2 solid-state Ka-band dual-polarization cloud radar provides radar reflectivity factor to drive the fog Vis retrieval algorithm. A DNQ3 Vis meter, integrated into an automatic observation platform, serves as the in-situ reference for validating the retrieved Vis. In addition, an FM-120 fog droplet spectrometer provides detailed measurements of droplet size distribution and microphysical properties, which supports algorithm development and sensitivity analysis.

The YLUKA2 MMCR, manufactured by Aerospace New Sky Technology, is installed at the highest point of DOB, with an antenna height of approximately 25 m above the ground. Operating in the Ka-band (34.5 GHz–35.5 GHz, with an adjustable center frequency), the radar adopts an advanced technical architecture that integrates solid-state transmission, dual-transmitter/dual-receiver linear polarization, and fully coherent pulse-Doppler technology. Its key performance specifications include a spatial resolution of 30 m, a maximum detection range of 30 km, a ground clutter suppression ratio of $\geq$42 dB, and a minimum detectable reflectivity factor of ≤ -30 dBz at 10 km. These capabilities ensure reliable detection of weak fog echoes. The radar's minimum detectable fog vertical height is determined by radar's minimum detection range (150 m), the antenna beamwidth of $0.39°$, the radar scanning elevation angle ($2°$) and the antenna height above the ground (25 m). This value is estimated as $150 \times \sin(2° - 0.39°/2) + 25 = 30.2$ m, enabling effective observation of near-surface fog structures while reduc-

https://doi.org/10.5194/egusphere-2026-1032
Preprint. Discussion started: 30 March 2026
© Author(s) 2026. CC BY 4.0 License.

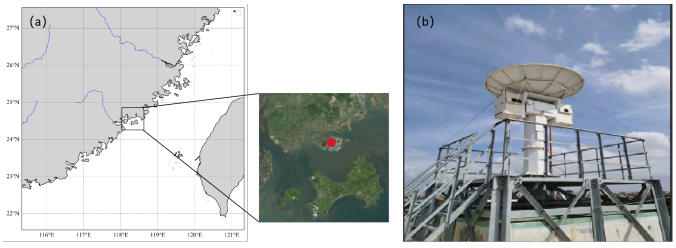

Figure 1. (a) Geographical location of DOB in Xiang'an District, Xiamen. Red mark denotes the position of the observation station. Map source: Baidu Maps, copyright © Baidu Inc., used for academic research only.

ing ground-clutter interference. Doppler and ground clutter suppression techniques are further employed to eliminate ground clutter effects due to antenna side lobes (Li et al., 2013; Kanemaru et al., 2021).

The FM-120 has been continuously running from 2019 through 2023. The FM-120 measures droplets with a size range of 2 µm–50 µm at a sampling frequency of 1 Hz, dividing measurements into 30 non-equidistant size bins. The DSD data acquired by the FM-120 are used to retrieve key fog microphysical parameters such as β_{ext}, LWC, and r_m, providing critical foundational data for algorithm development and systematic sensitivity analysis. The DNQ3 Vis meter, deployed on an automatic observation platform at DOB, operates based on the forward scattering principle. It emits infrared light pulses with a central wavelength of 0.87 µm via an infrared light-emitting diode. Scattered light at a 35° forward angle is received by the sensor and converted into electrical signals, which are subsequently processed to derive Vis. The DNQ3 Vis meter is located approximately 153 m from the radar along the 150° azimuth direction. To ensure consistency between MMCR and visibility measurement, collocation is performed by selecting the second valid radar range gate along the 150° azimuth, accounting for radar signal detection. Corresponding DNQ3 measurements from the same observation period are then used for matched analysis and algorithm validation.

3 Retrieval method

Vis (unit: m) is defined as the distance at which the contrast between an object and its background is reduced to 2% of its original value due to fog droplets extinction. This definition is grounded in the classical Koschmieder Law, developed in the 1920s (Horvath, 1971), which expresses Vis as:

$$\text{Vis} = -\frac{\ln \varepsilon}{\beta_{\text{ext}}} = -\frac{\ln 0.02}{\beta_{\text{ext}}} \tag{1}$$

where ε is the brightness contrast threshold. It represents the minimum contrast detectable by a standard observer with normal vision and is typically set to 0.02. β_{ext} is the extinction coefficient (unit: m^{-1}) at the visible light wavelength of 550 nm. According to Mie scattering theory, the β_{ext} is given by:

$$\beta_{\text{ext}} = \int_0^\infty Q_{\text{ext}}(r,\lambda) n(r) \pi r^2 \, \mathrm{d}r \tag{2}$$

https://doi.org/10.5194/egusphere-2026-1032
Preprint. Discussion started: 30 March 2026
© Author(s) 2026. CC BY 4.0 License.

where Q_{ext} is the extinction efficiency of droplets with radius r, quantified as the ratio of actual extinction cross-section to the geometric cross-section. Q_{ext} depends on both droplet radius r and incident wavelength. The function $n(r)$ denotes the fog droplet size distribution function (unit: m^4), typically assumed to follow a lognormal distribution (Bernardin et al., 2010; Podzimek, 1997):

$$n(r) = \frac{N_T}{\sqrt{2\pi}\, r\sigma} \exp\left[\frac{-\ln^2(r/r_m)}{2\sigma^2}\right] \tag{3}$$

where N_T is the total fog droplet number concentration, r_m is the geometric median radius, $r_m = \exp\left(\overline{\ln r}\right)$, and σ is the logarithmic spectral width, $\sigma = \sqrt{\overline{(\ln r - \ln r_m)^2}}$.

Based on lognormal distribution statistics, any k-th moment of DSD ($M_k = \int_0^\infty r^k n(r)\,\mathrm{d}r$) can be simplified to an analytical form:

$$M_k = N_T \exp\left(k\mu + \frac{k^2\sigma^2}{2}\right) = N_T\, r_m^k \exp\left(\frac{k^2\sigma^2}{2}\right) \tag{4}$$

Notably, MMCR operates in the millimeter wave band, where most fog droplets (2 μm–50 μm in diameter) fall within the Rayleigh scattering regime. Under this approximation, the radar scattering cross-section of an individual droplet scales with the 6th power of its diameter. As a volumetrically integrated parameter, the attenuation-corrected unattenuated radar reflectivity factor (Z, unit: $\mathrm{mm}^6/\mathrm{m}^3$; commonly representing the total backscattering from all droplets within the sampling volume) is mathematically expressed as the sixth-moment integral of DSD:

$$Z = 64M_6 = 64N_T r_m^6 \exp\left(18\sigma^2\right) \tag{5}$$

Both Z and β_{ext} are governed by different moments of the fog DSD, which precludes the establishment of a direct quantitative linkage between them. Therefore, we introduce two key fog microphysical parameters—LWC and r_e—both of which are also defined via DSD moments, to serve as intermediate variables for bridging Z and β_{ext}:

$$\mathrm{LWC} = \frac{4}{3}\pi\rho_w M_3 = \frac{4}{3}\pi\rho_w N_T r_m^3 \exp\left(\frac{9}{2}\sigma^2\right) \tag{6}$$

$$r_e = \frac{M_3}{M_2} = r_m \exp\left(\frac{5}{2}\sigma^2\right) \tag{7}$$

where ρ_w is the density of water, LWC is the mass of liquid water per unit volume of fog (unit: $\mathrm{g/m}^3$, a direct function of the 3rd DSD moment (M_3)), and r_e is the volume-weighted average fog droplet size (unit: μm, defined by the ratio of the 3rd to 2nd DSD moments (M_3/M_2)). It is clear that both LWC and r_e are fundamentally linked to the DSD and are derived from its statistical moments. Consequently, they implicitly incorporate the unmeasurable DSD parameters N_T and σ. By eliminating these two unmeasurable variables from Eqs. (4) - (6), r_e can be explicitly expressed as a function of LWC and Z (Stephens, 1978):

$$r_e = r_m^{\frac{4}{9}} \left(\frac{\pi\rho_w Z}{48\,\mathrm{LWC}}\right)^{\frac{5}{27}} \tag{8}$$

https://doi.org/10.5194/egusphere-2026-1032
Preprint. Discussion started: 30 March 2026
© Author(s) 2026. CC BY 4.0 License.

In the visible band (e.g., green light with a wavelength of ∼0.55 µm), fog droplet sizes are much larger than the incident wavelength, placing them within the scope of Mie scattering theory. For fog conditions, the extinction efficiency factor Q_{ext} can be approximated as 2 (Mazoyer et al., 2022). Substituting Eqs. (2), (6), (7) and (8) into the form of β_{ext} yields a closed-form relationship between β_{ext}, LWC and r_e:

$$\beta_{\mathrm{ext}} = \frac{3\mathrm{LWC}}{2r_e} = \frac{3}{2} r_m^{-\frac{4}{9}} \left(\frac{\pi \rho_w Z}{48}\right)^{-\frac{5}{27}} \mathrm{LWC}^{\frac{22}{27}} \tag{9}$$

For dimensional consistency in Eq. (9), LWC is converted to kg/m^3 and r_e to m during calculation, with the conversion relations being 1 g/m^3 = 10^{-3} kg/m^3 and 1 µm = 10^{-6} m. From the above derivations, the parameterization scheme for Vis can be expressed as:

$$\mathrm{Vis} = 3.912 \cdot \frac{2}{3} r_m^{\frac{4}{9}} \left(\frac{\pi \rho_w Z}{48}\right)^{\frac{5}{27}} \mathrm{LWC}^{-\frac{22}{27}} \tag{10}$$

In Eq. (9), both LWC and r_m are required for the calculation of Vis; however, neither parameter can be directly obtained from cloud radar measurement. Therefore, appropriate strategies are needed to express these variables in terms of radar-measurable quantities. Herein, LWC is first retrieved by applying an adaptive physical constraint derived from liquid water absorption attenuation, as developed in our previous work (Ge et al., 2023). The retrieved LWC is then used to correct the attenuated radar reflectivity (Z_m). Second, we exploit the microphysical coupling between r_m and intrinsic radar reflectivity Z to establish an empirical relationship linking these two variables. Through these two key steps, the physically constrained retrieval of LWC and the estimation of r_m are obtained for Vis inversion, while simultaneously completing the correction of radar signal attenuation caused by liquid water in fog. Based on this framework, we propose a self-consistent visibility retrieval algorithm, with the workflow summarized in the flowchart shown in Fig. 2.

3.1 LWC retrieval and radar reflectivity attenuation correction

In the Vis parameterization scheme, Vis inversion is inseparable from accurate LWC and unattenuated radar reflectivity factor Z. Therefore, we adopted the self-consistent LWC retrieval algorithm developed in Ge's research (Ge et al., 2023) to calculate LWC, and correct the absorption attenuation in the measured radar reflectivity Z_m. The attenuation of millimeter-wave radar signals during propagation in fog is mainly caused by mass absorption of water droplets; meanwhile, under the Rayleigh approximation, regardless of DSD, the proportional relationship between the absorption attenuation coefficient A and LWC (i.e., $A = K^*\mathrm{LWC}$) is adopted for LWC retrieval.

Through mathematical and physical transformation of the radar equation, a self-consistent relationship between the reconstructed measured radar reflectivity (Z_{mc}) and LWC was established as follows:

$$Z_{mc,r_i} = c\mathrm{LWC}_{r_i}^{\frac{1}{b}} \exp\left(-0.46 \int_{r_0}^{r_i} K^*\mathrm{LWC}(s)\,\mathrm{d}s\right) \tag{11}$$

Subsequently, the optimal parameters in the LWC expression for each radar range are obtained by minimizing the error between Z_m and the theoretically reconstructed reflectivity factor (Z_{mc}) expressed by Eq. (11). The trust region reflection (TRR)

https://doi.org/10.5194/egusphere-2026-1032
Preprint. Discussion started: 30 March 2026
© Author(s) 2026. CC BY 4.0 License.

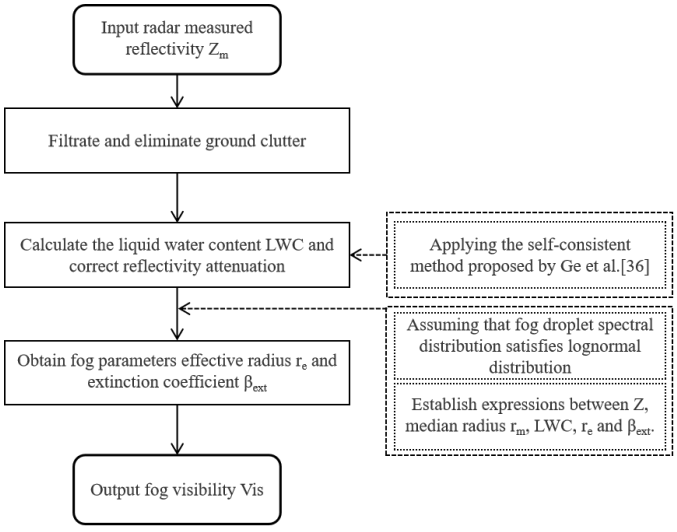

Figure 2. Flowchart of the Vis retrieval by our method. The framework of the overall algorithm is shown on the left; the method used to establish expressions between Z, median radius r_m, LWC, r_e, and β_{ext} under the lognormal droplet size distribution (DSD) assumption is shown in the dashed box on the right.

algorithm is employed to minimize the error function. This method breaks through the prior assumption of DSD in traditional algorithms, utilizes nonlinear least squares regression for parameter optimization, and enables accurate LWC inversion for liquid water clouds and fog. The accuracy of this algorithm has been verified by comparing the retrieved LWC with in-situ aircraft data and microwave radiometer products. Notably, there are differences between sea fog and clouds: the horizontal scale of sea fog typically ranges from several kilometers to tens of kilometers, far exceeding the vertical scale of clouds. The significant fluctuation in liquid water path (LWP) adversely affects the stability of the algorithm. To mitigate this impact, this study adopts the 10-bin segmentation method to divide continuous long-range fog echo data into several segments of 4–10 bin echo data (Zhang et al., 2024; Boers et al., 2013). This approach aligns the initial LWC range with previous studies, thereby reducing the number of iterations and calculation errors.

3.2 Relationship between r_m and Z

In addition to obtaining accurate LWC, determining r_m is also a critical step. Although some observational studies on r_m have been conducted previously, no empirical relationship between r_m and Z for fog has been established to date. Since both r_m and Z are closely related to DSD, a strong power-law correlation exists between them. Herein, we adopt the power function form $r_m = aZ^b$ to fit their relationship. The specific approach is as follows: combining Eqs. (3)–(6) and the DSD data observed by the FM-120 fog droplet spectrometer, the true values of fog microphysical parameters are calculated; based on Eq. (8), a residual formula is constructed by fitting the estimated β_{est} corresponding to different r_m values with the true values; finally, the fitting relationship $r_m = aZ^b$ is obtained through regression analysis. The results are shown in Fig. 3, with the fitted

https://doi.org/10.5194/egusphere-2026-1032
Preprint. Discussion started: 30 March 2026
© Author(s) 2026. CC BY 4.0 License.

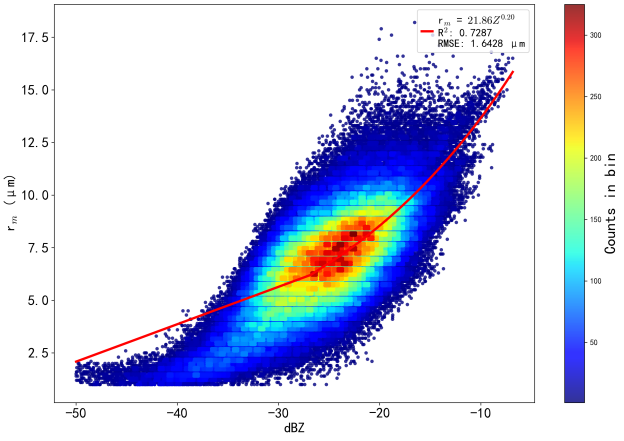

Figure 3. By minimizing the error between the estimated $\beta_{\mathrm{ext,est}}$ calculated from Eq. (9) and its true value β_{ext} calculated from Eq. (2), the power-law fitting relationship $r_m = 21.96Z^{0.2}$ was derived. This figure illustrates the relationship between the fitted r_m and Z. Herein, the abscissa represents Z (unit: dBz), and the ordinate denotes the fitted r_m (unit: μm). The red line denotes the fitted curve.

relationship being $r_m = 21.96Z^{0.2}$. At low Z values, the fitted r_m is significantly overestimated; however, considering that the main Z range of fog observed by radar is −40 dBz–−10 dBz (Du et al., 2024), this effect can be appropriately neglected.

4 Algorithm sensitivity analysis

There are two key uncertainties in algorithm construction that induce retrieval errors: the simplification of $Q_{\mathrm{ext}} \approx 2$ under Mie scattering theory, and potential deviations in retrieved LWC and empirically derived r_m. To quantify their respective impacts on β_{ext} (and thus indirect effects on Vis retrieval), we perform a systematic uncertainty analysis below.

4.1 Uncertainty from the $Q_{\mathrm{ext}} \approx 2$ approximation

For 550 nm electromagnetic waves, fog droplets are typically treated under Mie scattering theory. In this framework, Q_{ext} of large particles tends to 2—a simplification that introduces errors in practical calculations. For this purpose, error analysis is performed by combining Mie scattering theory with DSD data: Q_{ext} values for droplets of different sizes are calculated via Mie scattering theory, and these values are integrated with DSD measurements from the FM-120 fog droplet spectrometer to derive the accurate β_{ext}.

Figure 4 illustrates the variation of Q_{ext} with fog droplet radius (1 μm–25 μm) based on Mie scattering theory, where red dots represent Q_{ext} values corresponding to each size bin of the FM-120. To assess errors induced by the $Q_{\mathrm{ext}} \approx 2$ approximation, we compared two β_{ext} datasets: one approximated via the assumption ($\beta_{\mathrm{ext,appr}} = \int_0^\infty 2n(r)\pi r^2 \mathrm{d}r$) used in our algorithm, and the other accurately calculated from Eq. (2) via Mie scattering theory and FM-120 DSD data. Vis retrieved from these two β_{ext} datasets was compared to evaluate errors, using metrics including mean error (ME), mean absolute error (MAE), mean

https://doi.org/10.5194/egusphere-2026-1032
Preprint. Discussion started: 30 March 2026
© Author(s) 2026. CC BY 4.0 License.

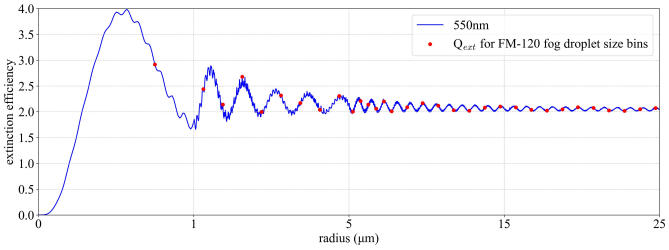

Figure 4. Relationship between Q_{ext} and fog droplet radius. Red dots represent Q_{ext} corresponding to each particle size bin of the FM-120 spectrometer.

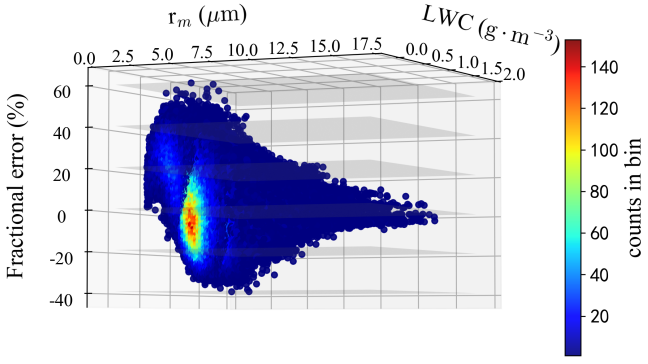

Figure 5. 3D histogram illustrating the relationship between fractional error of β_{ext} and two key fog microphysical parameters: r_m and LWC. All data points are derived from the 2019–2023 fog droplet spectrum observations collected by the FM-120 spectrometer at DOB.

squared error (MSE), and root mean squared error (RMSE). The results show an MAE of 18.12 m, an RMSE of 25.74 m, and a fractional error of 8.35%, indicating that the $Q_{\text{ext}} \approx 2$ approximation introduces a certain degree of error and thus affects visibility retrieval outcomes. After incorporating fog microphysical parameters into β_{ext} parameterization, we obtained its parameterization equation (Eq. (9)). We conducted an in-depth comparative analysis between this equation and the original β_{ext} calculation equation (Eq. (2)) based on Mie scattering theory (Fig. 5). The results show an average fractional error of 8.5% with no significant improvement, as the metric exhibits minimal variation. Given the strong correlation between LWC and r_m, the fractional errors of β_{ext} plotted against LWC and r_m on the x-y plane cluster around a single curve, with error values decreasing as LWC and r_m increase. Notably, for $r_m < 5\,\mu\text{m}$, the $Q_{\text{ext}} \approx 2$ approximation underestimates the extinction contribution of small fog droplets (actual $Q_{\text{ext}} > 2$), thereby increasing the relative deviation of the parameterized β_{ext} from the true value calculated via Mie scattering theory—this deviation further propagates to Vis retrieval. As fog droplet size increases, most β_{ext} errors fall within $\pm 20\%$, and the fractional error decreases progressively, confirming that small fog droplets are the primary error source for β_{ext} retrieval using Eq. (9). The MMCR's detection range covers $Z > -40\,\text{dBz}$, corresponding to a fitted r_m of 4.4 μm. Although the radar blind zone overlaps with the range of large errors, the algorithm maintains stable

https://doi.org/10.5194/egusphere-2026-1032
Preprint. Discussion started: 30 March 2026
© Author(s) 2026. CC BY 4.0 License.

performance. Specifically, MMCR is inherently less sensitive to fog droplets corresponding to geometric mean radii smaller than this reference value. Given that small droplets are the primary source of large β_{ext} retrieval errors, their weak influence on radar measurements effectively minimizes the propagation of such errors to the final retrieval results. For this reason, the algorithm will maintain robust performance in practical Vis retrieval applications.

4.2 Uncertainty from LWC and r_m deviations

In practical application of the algorithm, reliable retrievals of LWC, Z, and r_e are essential for accurate Vis calculation via Eq. (10). On one hand, the fog DSD does not strictly follow the lognormal distribution and may exhibit bimodal or multimodal characteristics, which introduces uncertainties into the calculation. On the other hand, both LWC and r_m are derived from Z—while Z is simultaneously corrected during LWC retrieval via the self-consistent algorithm, residual deviations between the retrieved LWC and its true value still exist. Additionally, the corrected Z is influenced by LWC, which further propagates uncertainties to r_m. Furthermore, r_m itself is an estimated parameter, with a RMSE of 1.64 μm as shown in the validation results (Fig. 3).

To quantify the impact of these uncertainties on algorithm performance, we conducted perturbation simulations on both the retrieved LWC and empirically derived r_m, with a focus on analyzing the resulting characteristics of retrieval errors. We define a sensitivity metric f that characterizes how retrieval errors respond to perturbations in these two parameters. The perturbed extinction coefficient ($\beta_{\text{ext,pert}}$) is calculated as follows:

$$\beta_{\text{ext,pert}} = \frac{3}{2}\alpha r_m^{-\frac{4}{9}} \left(\frac{\pi\rho_w Z}{48}\right)^{-\frac{5}{27}} \lambda \text{LWC}^{\frac{22}{27}} \tag{12}$$

where α and λ denote the perturbation multipliers for parameter scaling—values greater than 1 indicate parameter amplification, while values between 0 and 1 indicate parameter reduction. Specifically, α corresponds to the perturbation multiplier for r_m, and λ corresponds to the perturbation multiplier for LWC, with both multipliers ranging from 0.5 to 2.0. The range of α (for r_m) is derived from 5 years of empirical statistical analysis of DSD data collected by the FM-120 fog droplet spectrometer, while the range of λ (for LWC) is adopted from the findings of Ge et al. (2023). We conduct the subsequent sensitivity analysis using DSD data acquired from the FM-120 fog droplet spectrometer, with the sensitivity metric f (relative error of β_{ext}) defined as:

$$f = \frac{\beta_{\text{ext,pert}} - \beta_{\text{ext}}}{\beta_{\text{ext}}} \tag{13}$$

The f values correspond to the relative errors associated with different combinations of α (for r_m) and λ (for LWC), as visualized in Fig. 6. Specifically, a value of $0 < f < 1$ indicates that the retrieved β_{ext} (when LWC is scaled by λ and r_m is scaled by α) is systematically underestimated, whereas $f > 1$ indicates a systematic overestimation of β_{ext}. As shown in Fig. 6, the algorithm exhibits higher sensitivity to LWC variations: retrieval errors (quantified by f) exhibit an exponential dependence on LWC changes, but a linear dependence on r_m perturbations. When both LWC and r_m are either simultaneously overestimated or underestimated—i.e., when they increase or decrease proportionally in tandem—the f values remain within

https://doi.org/10.5194/egusphere-2026-1032
Preprint. Discussion started: 30 March 2026
© Author(s) 2026. CC BY 4.0 License.

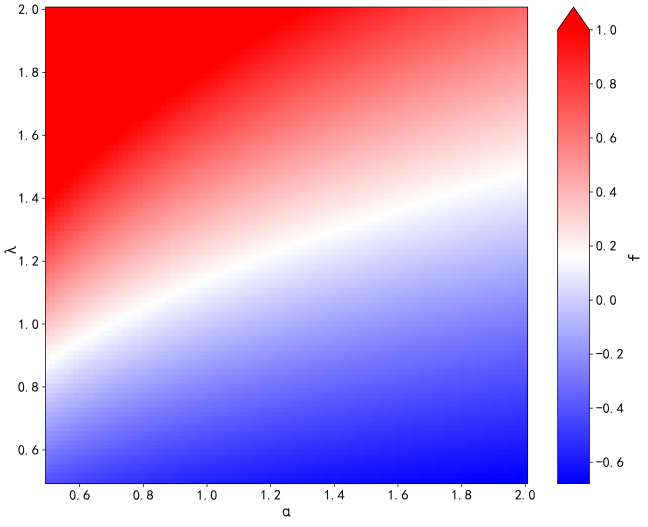

Figure 6. Sensitivity comparison of the algorithm to variations in LWC and r_m. The α represents the scaling factor for r_m (where $\alpha = 1$ denotes no scaling of r_m), and λ represents the scaling factor for LWC (where $\lambda = 1$ denotes no scaling of LWC).

a stable range. This confirms that the algorithm maintains reliable and stable performance even under coordinated variations of these two key microphysical parameters.

5 Application of algorithm in Vis retrieval

This algorithm was applied to the Ka-band radar installed at the DOB, with observations conducted in spring 2025 and subsequent analysis of retrieval results. A fog event observed at the Atmospheric Exploration Base on 2 March 2025, was selected as the research case. Influenced by the southern branch trough, this event formed when warm and humid southerly airflows passed through the observation site, classifying it as a typical advection sea fog. This advection sea fog developed with high density: it expanded rapidly after 18:00 local time and reached maximum intensity around 21:00. At a radar elevation angle of 2°, fog data could be detected up to a maximum distance of 10 km, with the fog top height exceeding 350 m. Between 18:00 and 24:00, Z generally decreased with increasing distance, indicating a stable fog structure with density decreasing with height. During 20:00–22:00, numerous data points with $Z > -10$ dBz were observed (peak values up to 0 dBz). As illustrated in Fig. 7, the high-Z regions are concentrated to the south and southwest of the observation site—areas where topographical undulations (e.g., hills) and man-made structures (e.g., buildings) are distributed.This indicates the high Z values are induced by the inhomogeneous underlying surface: the uneven surface generates turbulence, which in turn promotes droplet coalescence. This phenomenon is attributed to turbulence generated by friction between the fog and the nearby underlying surface, which induces droplet coalescence to form large droplets.

https://doi.org/10.5194/egusphere-2026-1032
Preprint. Discussion started: 30 March 2026
© Author(s) 2026. CC BY 4.0 License.

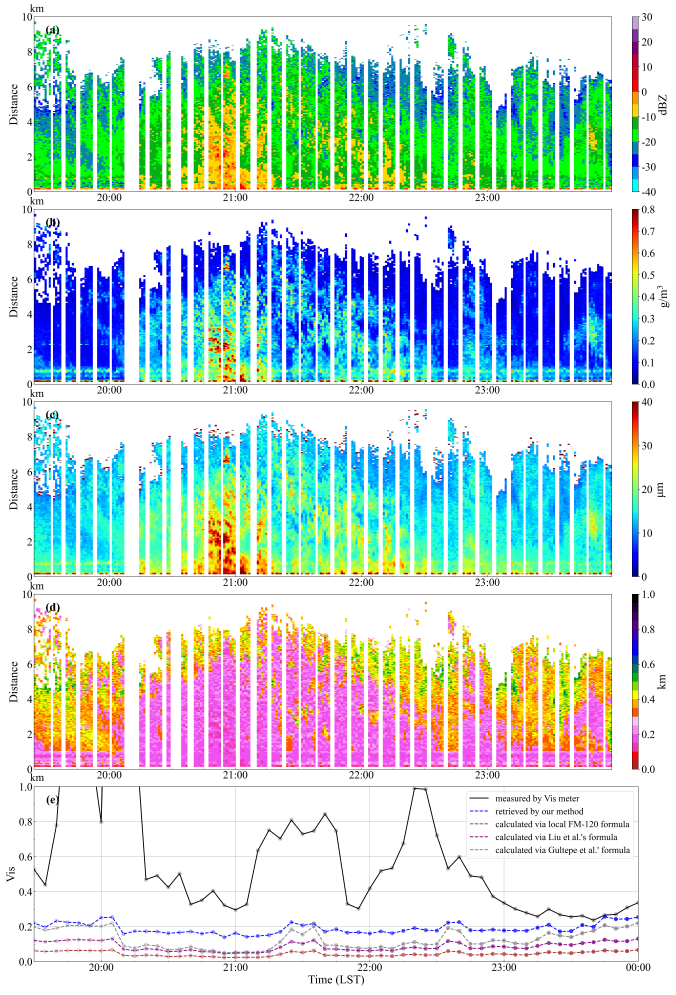

Figure 7. Application of the proposed algorithm to the advection fog case on 2 March 2025 (Local Standard Time, LST): (a) Reflectivity factor measured by the YLUKA2 MMCR; (b) LWC retrieved via the proposed algorithm; (c) r_e retrieved via the proposed algorithm; (d) Vis retrieved via the proposed algorithm; (e) Temporal variation of visibility during this event: the abscissa denotes time (LST), the ordinate represents visibility (unit: m); the black line corresponds to DNQ3 Vis meter measurements, while the blue line denotes visibility retrieved by the proposed algorithm. For reference, visibility results calculated via three empirical formulas are also plotted: brown (local empirical formula), purple (Liu's empirical formula), and gray (Gultepe's empirical formula).

https://doi.org/10.5194/egusphere-2026-1032
Preprint. Discussion started: 30 March 2026
© Author(s) 2026. CC BY 4.0 License.

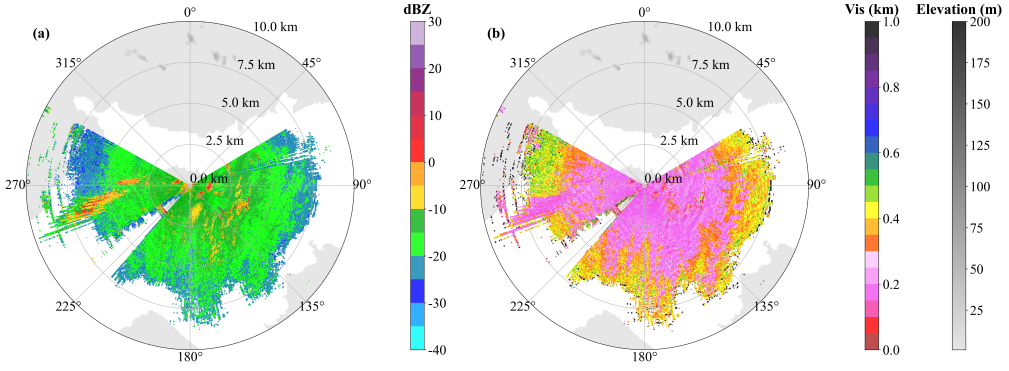

Figure 8. Polar radar scans at 20:29 (LST) on 2 March 2025: (a) Z_m, unit: dBz; (b) Retrieved visibility (Vis, unit: m; color represents Vis value, corresponding to right-side color bars).

To verify the rationality of algorithm parameter selection and estimate retrieval errors, the proposed method was cross-validated against Vis empirical algorithms from different regions and DNQ3 observations. To ensure the diversity of the comparison, three traditional Vis-Z empirical formulas derived from different regions were selected, which are listed as follows:Local empirical formula (derived from FM-120 observations): $\mathrm{Vis} = 20Z^{0.07}$; Liu Guangpu et al.'s formula (derived from synchronous radar-visibility meter data in Pingtan, Fujian): $\mathrm{Vis} = 40Z^{0.069}$ (Liu et al., 2019); Gultepe et al.'s relationship (derived from FMD-FM100 observations in Lunenburg): $\mathrm{Vis} = 40Z^{0.098}$ (Gultepe et al., 2006). As illustrated in Fig. 7(e), all methods exhibited consistent Vis variation trends. However, Vis retrieved from millimeter-wave radar data using different methods were lower than DNQ3 observations, with smaller temporal variability. Notably, at 21:00 LST, the radar-detected signal intensified while the DNQ3-measured Vis increased. This seemingly contradictory phenomenon stems from the combined effects of fog microphysical processes and instrument-specific limitations. On the one hand, droplet coalescence in the fog generates large particles, which reduces the total droplet number concentration and directly contributes to higher surface Vis. The DNQ3 is deployed at 1.5 m above the ground, whereas the radar operates at an approximate detection height of 30 m—this difference in observation heights causes large near-surface droplets to more easily adhere to surface objects (e.g., vegetation, structures), further enhancing the Vis measured by the ground-based DNQ3. On the other hand, as fog droplet diameter increases to values far exceeding the DNQ3's operating wavelength of 0.87 μm, the scattering behavior of the droplets transitions from Mie scattering to geometric optics scattering—resulting in a sharp decline in the DNQ3's sensitivity to these large droplets and an overestimation of surface Vis. In the presence of large fog droplets, there exists a systematic bias whereby MMCR-retrieved visibility is consistently lower than that measured by the DNQ3.

Statistical analysis was performed using ten sea fog events in spring 2025. Fig. 9 presents a comparison of Vis retrieved by the proposed algorithm (Fig. 9a) and three traditional empirical Vis-Z methods (Figs. 9b–d) against in-situ measurements from the DNQ3 forward-scattering Vis meter. The proposed algorithm yields a fractional error of 36.61%, versus 46.96% for the local FM-120 empirical formula, 38.61% for Liu et al.'s formula, and 77.08% for Gultepe et al.'s formula. From the perspective of retrieval accuracy, the Vis derived by our proposed algorithm shows the closest agreement with the in-situ DNQ3

https://doi.org/10.5194/egusphere-2026-1032
Preprint. Discussion started: 30 March 2026
© Author(s) 2026. CC BY 4.0 License.

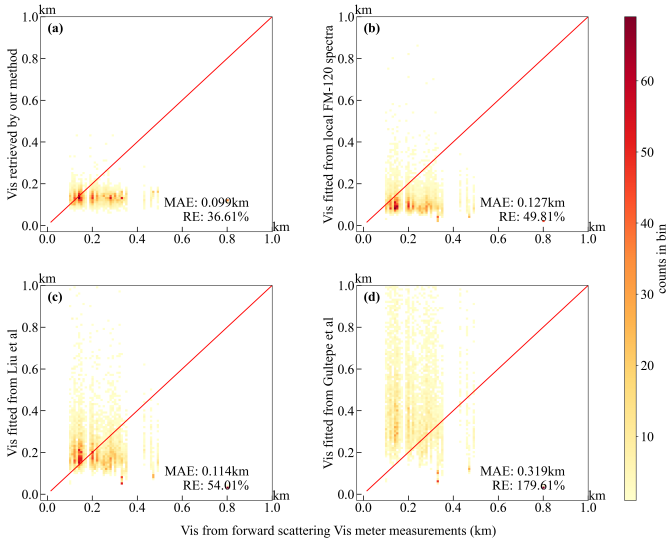

Figure 9. Evaluation of visibility retrieval results from different methods versus in-situ measurements from the DNQ3 forward-scattering visibility meter, for (a)–(d) distinct retrieval approaches: (a) Results from the proposed algorithm; (b) Results from the local empirical formula; (c) Results from the method of Liu et al.; (d) Results from the method of Gultepe et al. In all panels, the abscissa represents Vis from DNQ3 (unit: m), the ordinate represents Vis retrieved by the corresponding method (unit: m); and the grey dash line represents the same retrieved and in-situ Vis.

observations. It is followed by the local FM-120 formula and Liu et al.'s formula—both fitted based on observational data in Fujian Province—while Gultepe et al.'s formula (established from Lunenburg datasets) performs the poorest with the largest deviation. It is noteworthy that limited by the observation range of the FM-120 fog droplet spectrometer, variations in r_m cannot be fully captured in the fitting process when large fog droplets are present—leading to larger biases in the fitted r_m values. Although Sect. 4 identifies LWC as the primary factor influencing the algorithm, this r_m-related limitation still introduces a certain degree of impact. Despite the existence of systematic errors and limitations in formula fitting, the proposed algorithm still demonstrates superior stability and smaller retrieval errors compared to the traditional empirical methods—validating the excellent applicability of our method for Vis retrieval.

6 Conclusions

This study proposes a novel fog Vis retrieval algorithm based on single-band MMCR data, addressing the limitations of existing empirical methods and expanding the application of MMCR in fog remote sensing. The algorithm integrates radar transmission theory with fog microphysical properties that establishes a physically constrained framework to avoid reliance on empirical coefficients. By leveraging the intrinsic link between Z and β_{ext} through intermediate parameters LWC and r_m, the algorithm achieves superior adaptability across diverse fog regimes compared to traditional Vis-Z empirical methods. The algorithm also

https://doi.org/10.5194/egusphere-2026-1032
Preprint. Discussion started: 30 March 2026
© Author(s) 2026. CC BY 4.0 License.

exhibits higher sensitivity to LWC variations than to r_m perturbations, while coordinated proportional changes in LWC and r_m maintain retrieval stability by mitigating cumulative uncertainties. This method requires no auxiliary instruments, applies to diverse fog conditions, and has a fractional error of 8.35% induced by the $Q_{\text{ext}} \approx 2$ approximation (with small fog droplets as the primary error source); its overall retrieval fractional error (36.61%) outperforms traditional empirical algorithms.

Application to a typical advection sea fog event on 2 March 2025 demonstrates the algorithm's ability to capture the temporal and spatial variations of fog Vis. During the retrieval process, the algorithm's retrieval error is mainly influenced by LWC and r_m; notably, since both LWC and r_m are derived from Z, they tend to co-vary proportionally with changes in Z. This coordinated variation effectively mitigates the cumulative impact of individual parameter uncertainties, ensuring the algorithm maintains good stability even under fluctuating fog microphysical conditions. Statistical validation using 10 sea fog events shows the retrieval results exhibit good consistency and accuracy when compared to both classical empirical formulas and in-situ visibility meter observations, further confirming the algorithm's superior accuracy compared to three traditional empirical formulas—with its retrieved Vis values being closest to DNQ3 in-situ observations.

Overall, compared to traditional radar empirical coefficient algorithms, the proposed Vis retrieval method—built on the self-consistent LWC algorithm, attenuation-corrected reflectivity, and fog microphysical parameters—exhibits better adaptability and higher accuracy, and holds potential for Vis retrieval in various fog types. However, we also note due to certain assumptions in algorithm construction, previous studies have shown that fog often exhibits a bimodal DSD (Liu et al., 2025), and the specific impact of this phenomenon on the algorithm was not discussed here. Future work will further analyze the impact of bimodal DSD on the algorithm.

Code and data availability. The instrumental data used in this work are provided by the Key Innovation Team of Marine Severe Weather Mechanism and Forecasting, Fujian Meteorological Bureau. The intermediate variable data (including liquid water content, LWC; effective droplet radius, r_e) and the final visibility (Vis) retrieval program calculated from these variables, which are presented in this paper, are available upon reasonable request to the corresponding author(s).

Author contributions. Xiaojie Li developed the research concepts and methodology for fog visibility retrieval, performed formal statistical and computational analyses of radar data, conducted field investigations at the observation base, created data visualizations, and drafted the original manuscript. Jinming Ge contributed to the conceptualization of the study and refinement of the retrieval methodology, supervised the overall research process, acquired financial support for the project, managed project administration, provided key research resources, and reviewed and edited the manuscript (corresponding author). Yucheng Qiu curated and processed fog observation data, validated the retrieval algorithm results, and participated in field investigations. Qiaoyi Lv provided research resources, conducted field investigations, curated experimental data, and reviewed and edited the manuscript (corresponding author). Wei Song performed formal analysis of fog microphysical parameters and refined the retrieval methodology. Jie Zhang, Chi Zhang, Bochun Liu, Jiapeng Wang, Hongwei Xia, and Yuhang Zhu participated in field investigations, created visualizations of radar and visibility data, and curated the collected observation data. All authors read and approved the final version of the manuscript.

https://doi.org/10.5194/egusphere-2026-1032
Preprint. Discussion started: 30 March 2026
© Author(s) 2026. CC BY 4.0 License.

Competing interests. The authors declare that they have no conflict of interest.

Acknowledgements. The authors would like to extend their gratitude to the Key Innovation Team of Marine Severe Weather Mechanism and Forecasting, Fujian Meteorological Bureau, for providing valuable data, conducting fruitful discussions on research questions, and offering kind support in daily work.

Financial support. This research has been supported by the National Natural Science Foundation of China (grant nos. 42275076, 42427804) and the Research Project of Aerospace New Meteorological Technology Co., Ltd. (grant no. BW230315-015).

https://doi.org/10.5194/egusphere-2026-1032
Preprint. Discussion started: 30 March 2026
© Author(s) 2026. CC BY 4.0 License.

References

Antoine, S., Honnert, R., Seity, Y., Vié, B., Burnet, F., and Martinet, P.: Evaluation of an Improved AROME Configuration for Fog Forecasts during the SOFOG3D Campaign, *Wea. Forecasting*, 38, 1605–1620, doi:10.1175/WAF-D-22-0215.1, 2023.

Bell, A.: W-Band Radar Observations for Fog Forecast Improvement: an Analysis of Model and Forward Operator Errors, *Atmos. Meas. Tech.*, 14, 4929–4946, doi:10.5194/amt-14-4929-2021, 2021.

Bernardin, F., Colomb, M., Egal, F., Morange, P., and Boreux, J.: Droplet distribution models for visibility calculation, Tech. Rep., 2010.

Boers, R., Klein Baltink, H., Hemink, H. J., Bosveld, F. C., and Moerman, M.: Ground-Based Observations and Modeling of the Visibility and Radar Reflectivity in a Radiation Fog Layer, *J. Atmos. Oceanic Technol.*, 30, 288–300, doi:10.1175/JTECH-D-12-00081.1, 2013.

Claxton, B.: Vera: A stochastic, polydisperse scheme for diagnosing fog and visibility, *Q. J. Roy. Meteor. Soc.*, 151, e4915, doi:10.1002/qj.4915, 2025.

Cheng, X., Yang, B., Liu, G., Olofsson, T., and Li, H.: A Variational Approach to Atmospheric Visibility Estimation in the Weather of Fog and Haze, *Sustain. Cities Soc.*, 39, 215–224, doi:10.1016/j.scs.2018.02.001, 2018.

Duran-Rosal, A. M., Fernandez, J. C., Casanova-Mateo, C., Sanz-Justo, J., Salcedo-Sanz, S., and Hervas-Martinez, C.: Efficient Fog Prediction with Multi-Objective Evolutionary Neural Networks, *Appl. Soft Comput.*, 70, 347–358, doi:10.1016/j.asoc.2018.05.035, 2018.

Du, J., et al.: An Accurate Retrieval of Cloud Droplet Effective Radius for Single-Wavelength Cloud Radar, *IEEE Trans. Geosci. Remote Sens.*, 62, 4108511, doi:10.1109/TGRS.2024.3447002, 2024.

Eldridge, R. G.: Haze and Fog Aerosol Distributions, *J. Atmos. Sci.*, 23, 605–613, doi:10.1175/1520-0469(1966)023<0605:HAFAD>2.0.CO;2, 1966.

Ge, J., et al.: A Novel Liquid Water Content Retrieval Method Based on Mass Absorption for Single-Wavelength Cloud Radar, *IEEE Trans. Geosci. Remote Sens.*, 61, 4102815, doi:10.1109/TGRS.2023.3278735, 2023.

Gultepe, I., Müller, M. D., and Boybeyi, Z.: A New Visibility Parameterization for Warm-Fog Applications in Numerical Weather Prediction Models, *J. Appl. Meteorol. Climatol.*, 45, 1469–1480, doi:10.1175/JAM2423.1, 2006.

Gultepe, I., Tardif, R., Michaelides, S. C., Cermak, J., Bott, A., Bendix, J., Müller, M. D., Pagowski, M., Hansen, B., Ellrod, G., Jacobs, W., Toth, G., and Cober, S. G.: Fog Research: A Review of Past Achievements and Future Perspectives, *Pure Appl. Geophys.*, 164, 1121–1159, doi:10.1007/s00024-007-0211-x, 2007.

Gultepe, I., and Coauthors: The Fog Remote Sensing and Modeling Field Project, *Bull. Amer. Meteor. Soc.*, 90, 341–360, doi:10.1175/2008BAMS2354.1, 2009.

Guo, X., Wan, J., Liu, S., Xu, M., Sheng, H., and Yasir, M.: A scSE-LinkNet Deep Learning Model for Daytime Sea Fog Detection, *Remote Sens.*, 13, 5163, doi:10.3390/rs13245163, 2021.

Horvath, H.: On the applicability of the koschmieder visibility formula, *Atmos. Environ.*, 5, 177–184, doi:10.1016/0004-6981(71)90081-3, 1971.

Hu, S., Wang, Z., Zhang, X., et al.: Analysis of Sea Fog Echo Characteristics and Visibility Inversion of Millimeter-Wave Radar, *Meteorol. Monthly*, 48, 1270–1280, doi:10.7519/j.issn.1000-0526.2022.042601, 2022.

Jayakumar, A., Anurose, T. J., Bhati, S., Hendry, M. A., Hayman, G., Gordon, H., et al.: Development of an Integrated Modeling Framework for Visibility and Air Quality Forecasting in Delhi, *Bull. Am. Meteorol. Soc.*, 106, E261–E274, doi:10.1175/BAMS-D-24-0194.1, 2025.

Kamangir, H., Krell, E., Collins, W., King, S. A., and Tissot, P.: Importance of 3D convolution and physics on a deep learning coastal fog model, *Environ. Model. Softw.*, 154, 105424, doi:10.1016/j.envsoft.2022.105424, 2022.

https://doi.org/10.5194/egusphere-2026-1032
Preprint. Discussion started: 30 March 2026
© Author(s) 2026. CC BY 4.0 License.

Kanemaru, K., Hanado, H., and Nakagawa, K.: Improvement of the Clutter Removal Method for the Spaceborne Precipitation Radars, *IGARSS 2021*, 840–843, doi:10.1109/IGARSS47720.2021.9554974, 2021.

Leung, A. C. W., Gough, W. A., and Butler, K. A.: Changes in Fog, Ice Fog, and Low Visibility in the Hudson Bay region: Impacts on Aviation, *Atmosphere*, 11, 186, doi:10.3390/atmos11020186, 2020.

Li, Y., Zhang, G., Doviak, R. J., Lei, L., and Cao, Q.: A New Approach to Detect Ground Clutter Mixed With Weather Signals, *IEEE Trans. Geosci. Remote Sens.*, 51, 2373–2387, doi:10.1109/TGRS.2012.2209658, 2013.

Li, Y., Hoogeboom, P., and Russchenberg, H. W. J.: A Novel Radar-Based Visibility Estimator, *IEEE Trans. Geosci. Remote Sens.*, 55, 3150–3168, doi:10.1109/TGRS.2017.2662715, 2017.

Liu, D., Li, Z., Yan, W., and Li, Y.: Advances in fog microphysics research in China, *Asia-Pac. J. Atmos. Sci.*, 53, 131–148, doi:10.1007/s13143-016-0028-8, 2017.

Liu, G. P., Huang, S. Y., Liang, Y., et al.: Application of Millimeter Wave Radar in Harbor Marine Fog Observation and Visibility Inversion, *J. Arid Meteorol.*, 37, 993–1004, doi:10.11755/j.issn.1006-7639(2019)-06-0993, 2019.

Liu, Q., Shen, X., Sun, J., Zhang, Y., Qi, B., Ma, Q., Han, L., Xu, H., Hu, X., Lu, J., Liu, S., Yu, A., Liang, L., Gao, Q., Wang, H., Che, H., and Zhang, X.: Characterization of fog microphysics and their relationships with visibility at a mountain site in China, *Atmos. Chem. Phys.*, 25, 3253–3267, doi:10.5194/acp-25-3253-2025, 2025.

Long, Q., Wu, B., Mi, X., Liu, S., Fei, X., and Ju, T.: Review on Parameterization Schemes of Visibility in Fog and Brief Discussion of Applications Performance, *Atmosphere*, 12, 1666, doi:10.3390/atmos12121666, 2021.

Mazoyer, M., Burnet, F., and Denjean, C.: Experimental study on the evolution of droplet size distribution during the fog life cycle, *Atmos. Chem. Phys.*, 22, 11305–11321, doi:10.5194/acp-22-11305-2022, 2022.

Mahdavi, S., Amani, M., Bullock, T., and Beale, S.: Enhanced oceanic fog nowcasting through satellite-based recurrent neural networks, *Big Earth Data*, 9, 505–524, doi:10.1080/20964471.2024.2412379, 2024.

Miclea, R. C., Dughir, C., Alexa, F., Sandru, F., and Silea, I.: Laser and LIDAR in a System for Visibility Distance Estimation in Fog Conditions, *Sensors*, 20, 6322, doi:10.3390/s20216322, 2020.

Niu, S., Lu, C., Yu, H., et al.: Fog research in China: An overview, *Adv. Atmos. Sci.*, 27, 639–662, doi:10.1007/s00376-009-8174-8, 2010.

Podzimek, J.: Droplet Concentration and Size Distribution in Haze and Fog, *Studia Geophys. Geodaet.*, 41, 277–296, doi:10.1023/A:1023350917344, 1997.

Ran, Y., Ma, H., Liu, Z., Wu, X., Li, Y., and Feng, H.: Satellite Fog Detection at Dawn and Dusk Based on the Deep Learning Algorithm under Terrain-Restriction, *Remote Sens.*, 14, 4328, doi:10.3390/rs14174328, 2022.

Song, J. I., Yum, S. S., Gultepe, I., Chang, K. H., and Kim, B. G.: Development of a new visibility parameterization based on the measurement of fog microphysics at a mountain site in Korea, *Atmos. Res.*, 229, 115–126, doi:10.1016/j.atmosres.2019.06.011, 2019.

Stephens, G. L.: Radiation profiles in extended water clouds. II: Parameterization schemes, *J. Atmos. Sci.*, 35, 2123–2132, doi:10.1175/1520-0469(1978)035<2123:RPIEWC>2.0.CO;2, 1978.

Tjugum, S. A., Vaagen, J. S., Jakobsen, T., and Hamre, B.: Use of optical scatter sensors for measurement of visibility, *J. Environ. Monit.*, 7, 608–611, doi:10.1039/b414327b, 2005.

Ui, X., Lu, C. S., Yin, Y., et al.: Improved Visibility Diagnostic Scheme Based on Fog Microphysical Observation, *Chinese Journal of Atmospheric Sciences*, 47, 1375–1387, doi:10.3878/j.issn.1006-9895.2202.21138, 2023.

https://doi.org/10.5194/egusphere-2026-1032
Preprint. Discussion started: 30 March 2026
© Author(s) 2026. CC BY 4.0 License.

Zang, S., Ding, M., Smith, D., Tyler, P., Rakotoarivelo, T., and Kaafar, M. A.: The Impact of Adverse Weather Conditions on Autonomous Vehicles: How rain, Snow, Fog, and Hail Affect the Performance of a Self-Driving Car, *IEEE Veh. Technol. Mag.*, 14, 103–111, doi:10.1109/MVT.2019.2892497, 2019.

Zhang, W., Li, F., Lyu, Q., et al.: Comprehensive Analysis of a Sea Fog Event in Southern Coast of Fujian Based on Multi-Source Data, *Meteorol. Monthly*, 49, 682–696, doi:10.7519/j.issn.1000-0526.2023.011601, 2023.

Zhang, W., Cui, M., Wang, J., et al.: Statistical Characteristics of Droplet Spectrum and Their Relations with Visibility on Southern Coast of Fujian Province, *Chinese Journal of Atmospheric Sciences*, 48, 1978–1990, doi:10.3878/j.issn.1006-9895.2304.22088, 2024.

Zhou, Q., Fan, C., Han, Y., Su, D., Dong, L., and Zhang, Y.: Development of a New Intelligent Instrument for Visibility and Turbulence Meteorological Environment Parameters in Traffic Network, *Opt. Lasers Eng.*, 177, 108123, doi:10.1016/j.optlaseng.2024.108123, 2024.